THE JOURNAL OF BIOLOGICAL CHEMISTRY VOL. 287, NO. 30, pp. 24873–24883, July 20, 2012


# Headless Myo10 Is a Negative Regulator of Full-length Myo10 and Inhibits Axon Outgrowth in Cortical Neurons*[S]

Received for publication, April 4, 2012, and in revised form, May 25, 2012 Published, JBC Papers in Press, May 31, 2012, DOI 10.1074/jbc.M112.369173

**Alexander N. Raines**[‡§], **Sarbajeet Nagdas**[¶], **Michael L. Kerber**[¶], **and Richard E. Cheney**[§¶1]

*From the* [‡]*Curriculum in Neurobiology,* [§]*Neuroscience Center, and* [¶]*Department of Cell and Molecular Physiology, University of North Carolina at Chapel Hill, Chapel Hill, North Carolina 27599*

**Background:** A "headless" Myo10 that lacks a motor domain has been identified in the nervous system, but its functions are unknown.
**Results:** Headless Myo10 inhibits axon outgrowth and antagonizes the filopodia-inducing activity of full-length Myo10.
**Conclusion:** Full-length Myo10 is required for axon outgrowth, and headless Myo10 can inhibit full-length Myo10.
**Significance:** This study establishes opposing roles for headless and full-length Myo10 in axon outgrowth.

**Myo10 is an unconventional myosin that localizes to and induces filopodia, structures that are critical for growing axons. In addition to the ~240-kDa full-length Myo10, brain expresses a ~165 kDa isoform that lacks a functional motor domain and is known as headless Myo10. We and others have hypothesized that headless Myo10 acts as an endogenous dominant negative of full-length Myo10, but this hypothesis has not been tested, and the function of headless Myo10 remains unknown. We find that cortical neurons express both headless and full-length Myo10 and report the first isoform-specific localization of Myo10 in brain, which shows enrichment of headless Myo10 in regions of proliferating and migrating cells, including the embryonic ventricular zone and the postnatal rostral migratory stream. We also find that headless and full-length Myo10 are expressed in embryonic and neuronal stem cells. To directly test the function of headless and full-length Myo10, we used RNAi specific to each isoform in mouse cortical neuron cultures. Knockdown of full-length Myo10 reduces axon outgrowth, whereas knockdown of headless Myo10 increases axon outgrowth. To test whether headless Myo10 antagonizes full-length Myo10, we coexpressed both isoforms in COS-7 cells, which revealed that headless Myo10 suppresses the filopodia-inducing activity of full-length Myo10. Together, these results demonstrate that headless Myo10 can function as a negative regulator of full-length Myo10 and that the two isoforms of Myo10 have opposing roles in axon outgrowth.**

Nervous system development requires the precise outgrowth of axons to their targets, a process that depends on the growth cone. Growth cones are specialized protrusive structures studded with filopodia, finger-like protrusions with an actin core that sample the surrounding tissue for guidance cues and transform these signals into directed outgrowth. Myosin-X (Myo10) is an unconventional myosin that has critical functions in filopodia (1). Myo10 localizes to the tips of filopodia (2–6), moves within filopodia (6–10), and induces the formation of filopodia (4, 6, 7, 10, 11). Given the importance of filopodia in neuronal development, particularly in axon outgrowth and branching (12–15), Myo10 is likely to have critical functions in neuronal development. Myo10 may also participate in nerve regeneration, as it is up-regulated 7-fold in peripheral neurons during recovery from axotomy (16).

The tail region of Myo10 contains a unique array of domains reported to bind to molecules with prominent roles in neuronal function. A region containing three pleckstrin homology (PH) domains can bind phosphatidylinositol (3,4,5)-triphosphate and interact with the plasma membrane (4, 17), and Myo10 functions downstream of PI3K in macrophage phagocytosis (18). Recently, phosphatidylinositol (3,4,5)-triphosphate binding was shown to convert Myo10 from a compact, autoinhibited monomer to an active dimer (5), demonstrating that Myo10 motor activity can be regulated by the PI3K pathway. The myosin tail homology 4 (MyTH4) domain of Myo10 can bind microtubules and is required for proper spindle formation (19–23). By binding both actin and microtubules, Myo10 may mediate actin-microtubule interactions, which are important for axon outgrowth and branching (13, 24–26). The Myo10 tail region ends in a band4.1/ezrin/radixin/moesin (FERM) domain that can interact with $\beta$-integrins (27), positioning Myo10 to act as a molecular link between filopodial actin and the extracellular matrix.

The FERM domain of Myo10 can also bind to deleted in colorectal carcinoma (DCC)[2] and neogenin, receptors for the guidance molecule netrin (23, 28, 29). Myo10 is required for the distribution of DCC to the periphery (28), whereas DCC and neogenin have different effects on the type of filopodia induced by Myo10 (6). In the chicken spinal cord, shRNA to Myo10 impaired crossing of commissural axons across the midline (28), although it is not clear whether this defect resulted from incorrect guidance or insufficient outgrowth. Overexpression

* This work was supported, in whole or in part, by National Institutes of Health Grant R01 DC03299 (to R. E. C.). This work was also supported by Medical Science Training Program Grant T32GM008719 (to A. N. R.).
[S] This article contains supplemental Figs. S1–S3.
[1] To whom correspondence should be addressed: Department of Cell and Molecular Physiology, University of North Carolina at Chapel Hill, 111 Mason Farm Rd., Chapel Hill, NC. Tel.: 919-966-0331; Fax: 919-966-6927; E-mail: richard_cheney@med.unc.edu.

[2] The abbreviations used are: DCC, deleted in colorectal carcinoma; E15, embryonic day 15; P19, postnatal day 19; aa, amino acids; RMS, rostral migratory stream; PH, pleckstrin homology; MyTH4, myosin tail homology 4; FERM, band4.1/ezrin/radixin/moesin.

of a motorless Myo10 construct also inhibited commissural axon crossing (28).

Although motorless Myo10 constructs have been used as presumed dominant negatives (18, 28, 30), brain uses an alternate transcription start site to endogenously express a similar isoform, termed "headless" Myo10 (31). This headless Myo10 is missing most of the motor domain and thus lacks the key functional characteristic of a myosin: the ability to bind to actin filaments and exert force. Unlike the full-length protein, headless Myo10 does not localize to filopodial tips and does not undergo intrafilopodial motility (9, 31). Although headless Myo10 is hypothesized to act as an endogenous dominant negative (31), this hypothesis has never been tested directly.

Here we show that both full-length and headless Myo10 are expressed in embryonic mouse cortex and cultured cortical neurons. Surprisingly, headless Myo10 is also expressed in neural stem cells, and *in situ* hybridization reveals that headless Myo10 is most prominently expressed in the embryonic ventricular zone. We also report the first specific knockdown of headless Myo10, which significantly increases the outgrowth of axons of cultured cortical neurons. Knockdown of full-length Myo10 has the opposite effect, inhibiting axon outgrowth. We also demonstrate that headless Myo10 antagonizes the induction of filopodia by full-length Myo10, showing that headless Myo10 can indeed function as a dominant negative.

## EXPERIMENTAL PROCEDURES

*Animals*—Mice were used according to a protocol approved by the Institutional Animal Care and Use Committee at the University of North Carolina at Chapel Hill and in accordance with National Institutes of Health guidelines. Time-pregnant females were obtained from Charles River Laboratories.

*Ex Vivo Electroporation and Dissociated Cortical Neuron Cultures*—Mouse cortical progenitors were electroporated *ex vivo* at embryonic day 15 (E15) and cultured as described previously (32, 33). Embryos were harvested from time-pregnant BALB/c mice and decapitated in ice-cold Hanks' balanced salt solution (Invitrogen) with 2.5 mM Hepes (pH 7.4), 30 mM D-glucose, 1 mM $CaCl_2$, 1 mM $MgSO_4$, 4 mM $NaHCO_3$. Endotoxin-free plasmid plus 0.5% Fast Green (Sigma) was injected into the lateral ventricles using a PicoSpritzer III (General Valve) microinjector. The whole head was electroporated using an ECM 830 electroporator with gold-plated electrodes (GenePads 5 × 7 mm, BTX). Immediately after electroporation, the brain was removed, and the cortices dissected in ice-cold complete Hanks' balanced salt solution. The cortices were dissociated using papain and cultured on glass-bottom dishes (MatTek) coated with poly-L-lysine and laminin (Sigma) in serum-free medium (Neurobasal with 1% penicillin/streptomycin, L-glutamine, and B27 and N2 supplements, Invitrogen).

*Cell Culture and Transfection*—Cell culture reagents were obtained from Invitrogen unless noted otherwise. Neural stem cells were cultured as neurospheres from E15 cortex (34). The cortices were dissected and dissociated as described above and then cultured in Neurobasal medium with 1% penicillin/streptomycin, L-glutamine, B-27 and N-2 supplements, epidermal growth factor, and basic fibroblast growth factor. Astrocytes were cultured from E17 rat embryos and subcultured at 13 days *in vitro* at ~100,000 cells/$cm^2$. The glioblastoma cell lines U-87 and U-138 were maintained in Eagle's minimum essential medium with 0.1 mM non-essential amino acids, 1 mM sodium pyruvate, 10% FBS, 1% penicillin/streptomycin. P19 embryonal carcinoma cells were cultured in DMEM plus 10% FBS and 1% penicillin/streptomycin. COS-7 cells were maintained in DMEM plus 10% FBS and 1% penicillin/streptomycin. COS-7 cells were transfected using Lipofectamine 2000 (Invitrogen) according to the specifications of the manufacturer.

*Tissue Samples and Immunoblotting*—Tissue samples were flash-frozen in liquid nitrogen and stored at −80 °C until all samples were collected. The samples were then homogenized at full speed for ~30 s (Omni TH, Omni International) on ice in 10 ml/g of homogenization buffer (40 mM Hepes, 10 mM K-EDTA, 5 mM ATP, 2 mM DTT, 2× EDTA-free complete protease inhibitor mixture (pH 7.7), Roche Diagnostics). For cellular lysates, cultured neurons were scraped from the dish into ice-cold lysis buffer (40 mM Hepes (pH 7.4), 75 mM KCl, 2 mM K-EGTA, 1% Triton X-100, 2.5 mM $MgCl_2$, 5 mM ATP, 2 mM DTT, 2× EDTA-free complete protease inhibitor). Neurosphere cultures of neural stem cells were centrifuged, rinsed with PBS, and resuspended in ice-cold lysis buffer, whereas all other cell types were trypsinized before centrifuging, rinsing, and resuspending in ice-cold lysis buffer. Lysates were passed through a 27.5-gauge syringe 6 times to shear DNA, combined with $1/4^{th}$ volume SDS sample buffer (5× stock: 300 mM Tris-HCl, 10% SDS, 50% glycerol, 0.04% bromphenol blue, 50 mM DTT (pH 6.8)), and immediately heated at 95 °C for 5–10 min.

All samples were run on NuPAGE 4–12% Bis-Tris gels in NuPAGE MOPS SDS running buffer with the Novex Xcell SureLock mini-cell system (Invitrogen) at 120 V for 100 min. The gels were transferred onto nitrocellulose membranes (GE Water and Purification Technologies) with the Novex mini-cell system at 30 V for 3 h at 4 °C. The membranes were blocked for 1 h in 5% milk (Carnation nonfat instant dry milk, Nestle) in TBST (50 mM Tris (pH 7.5), 150 mM NaCl, 0.05% Tween 20). Primary antibodies were diluted in blocking solution to a final concentration of 1 μg/ml of rabbit anti-Myo10 antibody (Sigma, catalog no. HPA024223, made to amino acids 901–1047 of human Myo10) and 0.5 μg/ml of mouse monoclonal anti-actin antibody (Millipore, MAB1501R) as a loading control and incubated overnight at 4 °C. After washing 3 times with TBST, the membranes were incubated for 1 h with secondary antibodies (Rockland, goat anti-rabbit IRDye700Dx, goat anti-mouse IRDye800Dx) diluted 1:10,000 in blocking solution for a final concentration of 0.1 ng/ml. The membranes were then washed once with TBST and 3 times with TBS before imaging with a LiCor Odyssey infrared imaging system.

*Immunoprecipitation and Protein Sequencing*—Immunoprecipitation of Myo10 was carried out using a Dynabeads coimmunoprecipitation kit with M-270 epoxy beads (Invitrogen) following the protocol of the manufacturer. Briefly, 7.5 mg of beads were covalently coupled to 75 μg of affinity-purified rabbit anti-Myo10 antibody 505, which was raised against amino acids 808–917 of mouse Myo10, by overnight incubation at 37 °C. Brain tissue (1 g) from P10 mice was then harvested and homogenized in 5 ml of homogenization buffer as described above. The homogenate was centrifuged for 20 min at 50,000

rpm at 4 °C in a tabletop ultracentrifuge (Beckman-Coulter). The supernatant was divided into two aliquots and incubated with either non-immune control or Myo10 antibody-coupled beads on a rotator for 1 h at 4 °C. The beads were washed with 200 μl of homogenization buffer 3 times, once with 200 μl of the Dynal 1× last wash buffer, and transferred to a new tube. The beads were resuspended in 60 μl 1× PBS, combined with 15 μl of SDS sample buffer, and heated at 95 °C for 5 min. The samples were run on a 4–12% Bis-Tris gel as described above.

The Coomassie Blue-stained bands at ~240 kDa and ~165 kDa were excised from the gel, and in-gel trypsin digest was performed using a ProGest protein digestion station (Digilab®). The extracted peptides were first mixed with matrix (α-cyano-4-hydroxycinnamic acid), spotted onto a MALDI plate, and analyzed using a 4800 "Plus" MALDI-TOF/TOF mass spectrometer. The spectra were searched using MASCOT (Matrix Science, version 2.3.02) to confirm that each sample contained peptides from Myo10.

The extracted peptides were then loaded onto a 2-cm long × 360 μm outer diameter × 100 μm inner diameter microcapillary fused silica precolumn packed with Magic 5-μm C18AQ resin (Michrom Biosciences, Inc.). After sample loading, the precolumn was washed with 95% solvent A (0.1% formic acid in water)/95% solvent B (0.1% formic acid in acetonitrile) for 20 min at a flow rate of 2 μl/min. The precolumn was then connected to a 360 μm o.d. × 75 μm i.d. analytical column packed with 14 cm of 5 μm of C18 resin constructed with an integrated electrospray emitter tip. The peptides were eluted at a flow rate of 250 nL/min by increasing the percentage of solvent B to 40% with a Nano-Aquity HPLC solvent delivery system (Waters Corp.). The LC system was directly connected through an electrospray ionization source interfaced to an LTQ Velos ion trap mass spectrometer (Thermo Electron Corp.). The mass spectrometer was controlled by Xcalibur software (Thermo, version 2.1.0.1140) and operated in the data-dependent mode in which the initial MS scan recorded the mass to charge ($m/z$) ratios of ions over the range 400–2000. The 10 most abundant ions were automatically selected for subsequent collision-activated dissociation. Raw files were searched using MASCOT (Matrix Science, version 2.3.02) via Proteome Discoverer (Thermo, version 1.3.0.339) against the sequence for mouse myosin-X (NP_062345). Search parameters included peptide mass tolerance of 10 ppm, fragment ion tolerance of 0.8 mass unit, variable modifications for methionine oxidation, and no enzyme specificity. Peptides with an expectation value of less than 0.01 were considered "high confidence" matches.

*In Situ Hybridization*—Riboprobes to Myo10 were cloned into the pBluescript (pBS) vector. The tail probe was described previously (2) and corresponds to nucleotides 4862–5246 of mouse Myo10 mRNA (NM_019472). The head probe (AR4-1) was cloned from mouse Myo10 cDNA and corresponds to nucleotides 1245–1739 of NM_019472. The headless probe (AR4-2) consists of all 115 nucleotides of the predicted 5′ UTR of headless Myo10 and was synthesized directly and ligated into pBS.

Embryos or brains were fixed overnight in RNase-free 4% paraformaldehyde in 1× PBS at 4 °C. Tissue samples were rinsed in PBS and cryoprotected by immersion through sucrose (10 and 30% sucrose in RNase-free 1× PBS, each step overnight at 4 °C), embedded in freezing compound, rapidly frozen on dry ice, and stored at −80 °C. Serial cryosections were collected onto slides (Fisher Superfrost Plus) at 16-μm intervals and stored at −80 °C before *in situ* hybridization. After proteinase K pretreatment and prehybridization, 1–2 mg/ml digoxigenin-labeled riboprobes were hybridized for 12–16 h at 65 °C. After rinsing, sections were incubated with a 1:2000 dilution of alkaline phosphatase-conjugated sheep anti-digoxigenin (Roche) in blocking buffer for 3 h at room temperature and developed in a nitroblue tetrazolium/5-bromo-4-chloro-3-indolyl phosphate solution (20 μl/ml, Roche) in the dark overnight. After developing, sections were mounted in aqueous mounting medium (DAKO Faramount).

*Imaging and Quantification*—To analyze axon outgrowth, cultured neurons were fixed after 7 days *in vitro* in 4% paraformaldehyde in PBS for 20 min at room temperature and counterstained with β-tubulin III (Covance) to confirm neuronal identity. The neurons were imaged on a Nikon TE-2000 microscope with a 20× lens. All processes of the neuron were traced using the ImageJ plugin NeuronJ, and analyzed with XLNJ_Calculations, a Java program that performs batch analysis of NeuronJ tracing data (35). For quantification of filopodia number, COS-7 cells were replated 2 h after transfection onto poly-L-lysine-coated coverslips. The following morning, the cells were fixed 20 min in 4% paraformaldehyde in PBS, permeabilized with 0.05% Triton X-100 for 20 min, and stained with DAPI (200 nM) for 30 min. Individual, non-dividing, well isolated cells were then imaged on a Nikon TE-2000 microscope at ×60, and all peripheral filopodia were counted as described previously (7). Filopodia were defined as thin protrusions extending at least 0.75 μm.

*Constructs*—shRNA constructs were cloned into pSCV2, a bicistronic vector expressing shRNA under the RNA polymerase III-specific U6 promoter and Venus under the RNA polymerase II-specific chicken β-actin promoter (36). Using the Dharmacon siDesign Center, we selected the following targets: full-length Myo10 shRNA #1 (AR2-1), GCAATGCGAAGACAGTATA (nucleotides 1083–1101 of NM_019472 (37)); full-length Myo10 shRNA #2 (AR2-6), GAGGAAGAATTGTAGATTA (nucleotides 1170–1188); headless Myo10 shRNA #1 (AR2–3), CAGCATCTGAAGAGAGGAA (nucleotides 84–102 of the 5′ UTR); and headless Myo10 shRNA #2 (AR2–2), TGAAGAGAGGAAAGGGAAA (nucleotides 91–109 of the 5′ UTR). Results with AR2-1 and AR2-3 in Fig. 3 were confirmed with AR2-6 and AR2-2 in supplemental Fig. S2.

The following fluorescently tagged Myo10 constructs from bovine Myo10 in pEGFP-C2 (Clontech) have been described previously (7): GFP-full-length Myo10 (aa 1–2052 of bovine Myo10 sequence U55042), GFP-headless Myo10 (aa 644–2052), and GFP-Myo10 tail (aa 1160–2052). Bovine GFP-Myo10 α-helical region (aa 811–946) was generated by PCR and cloned into pEGFP-C3. Bovine mCherry-full-length Myo10 (MK1) was generated in a pEGFP-C2 modified to express mCherry instead of EGFP. Bovine GFP-full-length Myo10 (AR1-1) and GFP-headless Myo10 (AR1-2) were also cloned into the pCIG2 vector, which contains a (cDNA)-IRES-EGFP cassette under the control of a CMV

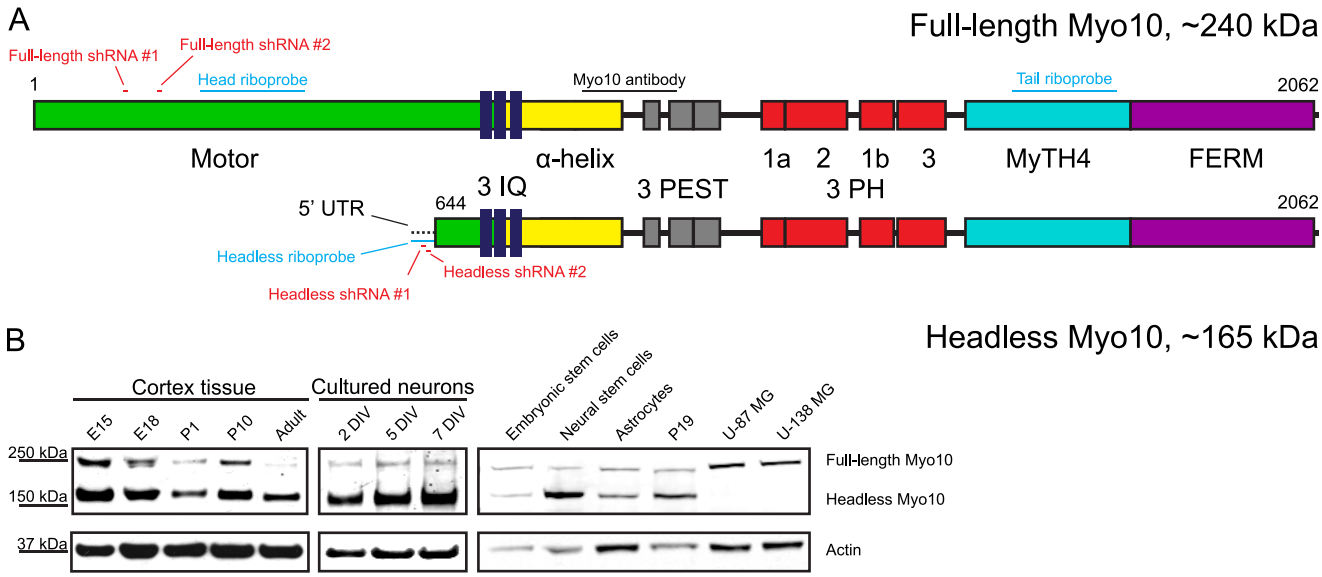


FIGURE 1. **Full-length and headless Myo10 are expressed in embryonic cortical neurons.** *A*, domain representation of the mouse sequence of full-length (NCBI, NP_062345.2) and headless Myo10 showing the recognition sequence of the anti-Myo10 antibody (Sigma, HPA024223), riboprobes (*blue*) and RNAi targets (*red*) used in this study. For the purposes of illustration, the ~115-bp 5′ UTR of headless Myo10 is included. Amino acid numbers are shown for the beginning and end of each protein. *IQ*, IQ motifs; *PEST*, region enriched in proline, glutamine, serine, and threonine; *PH*, pleckstrin homology domain; *MyTH4*, myosin tail homology 4 domain; *FERM*, band 4.1/ezrin/radixin/moesin domain. *B*, immunoblotting of cortical tissue and cultured cells reveals expression of both isoforms. Both headless and full-length Myo10 are also expressed in embryonic stem cells, neural stem cells, astrocytes, and multipotent P19 cells, but, like most cells, the glioblastoma cell lines U-87 and U-138 only express full-length Myo10.

enhancer and a chicken β-actin promoter (38). Mouse GFP-full-length Myo10 (aa 1–2062 of NP_062345), cloned into the BglII and KpnI sites of pEGFP-C3, was a generous gift of Erich Boger and Tom Friedman. Mouse headless Myo10 (aa 644–2062 and the entire 115-bp 5′ UTR) was cloned into pCIG2 by replacing the sequence for aa 1–643 with a synthetic fragment containing the 5′ UTR (AR1-3).

## RESULTS

*Full-length and Headless Myo10 Are Expressed in Cortical Neurons*—Two isoforms of Myo10 are detected in the brain (31), as diagrammed in Fig. 1*A*. Full-length Myo10 is expressed ubiquitously but at low levels in most cells and tissues (2), whereas headless Myo10 has only been identified in the nervous system, and its function is unknown. To confirm the initiation site of the headless Myo10 protein, we immunoprecipitated and sequenced both headless and full-length Myo10 from P10 mouse brain. The resulting peptides are within amino acids 190–2046 for full-length Myo10 and 645–2046 for headless Myo10. We also detect a single non-tryptic peptide from headless Myo10 that starts at Pro-645, strongly suggesting that the major form of headless Myo10 indeed initiates at Met-644, as predicted, then is processed by aminopeptidase cleavage of the initiating methionine, leaving amino acids 645–2062 (supplemental Fig. S1).

Although we showed previously that headless and full-length Myo10 are developmentally regulated in the postnatal mouse brain (31), little is known about the prenatal expression of Myo10. Immunoblotting of mouse cortical tissue (Fig. 1*B*) reveals that expression levels of both headless and full-length Myo10 are highest at E15. In cortex, both isoforms decrease at E18 and again at P1, resurge at P10, and then fade in adulthood. This is consistent with our previous results showing a peak of expression in whole cerebrum between P5 and P15 but low levels of expression before or after (31). Interestingly, headless Myo10 is the predominant isoform in mouse cortex at all time points (Fig. 1*B*).

Headless Myo10 is also the predominant isoform in cultured cortical neurons, whereas full-length Myo10 is expressed at lower levels (Fig. 1*B*). Immunoblotting also demonstrates that both full-length and headless Myo10 are expressed in embryonic stem cells, neural stem cells, and astrocytes. Both isoforms are also expressed in P19 cells, a multipotent embryonic carcinoma cell, but, like most cells, the glioblastoma cell lines U-87 and U-138 appear to express only full-length Myo10 (Fig. 1*B*).

*In Situ Hybridization Reveals Differential Localization of Full-length and Headless Myo10*—Previous efforts to determine the localization of Myo10 in brain have utilized antibodies or riboprobes that cannot distinguish between full-length and headless Myo10 (2, 31, 39–41). Because the protein sequence of headless Myo10 initiates at amino acid 644 but thereafter is identical to full-length Myo10, generation of a headless-specific antibody is unlikely. However, headless Myo10 is transcribed from an alternate start site, giving it a unique 5′ UTR of ~115 nucleotides (31). We used this 5′ UTR to generate a riboprobe for headless Myo10, which, along with probes to the head and tail of Myo10 (diagrammed in Fig. 1*A*), allowed us to determine the localization of each isoform. Sense control probes confirmed the absence of nonspecific labeling (data not shown). In coronal sections of E15 embryos, the tail probe, which should recognize transcripts of both isoforms, shows strong labeling in the ventricular zone (Fig. 2, *A* and *B*), the location of neurogenesis and gliogenesis in the developing brain. This is consistent with data from an *in situ* hybridization database using a probe to the tail of Myo10, which showed expression primarily in the

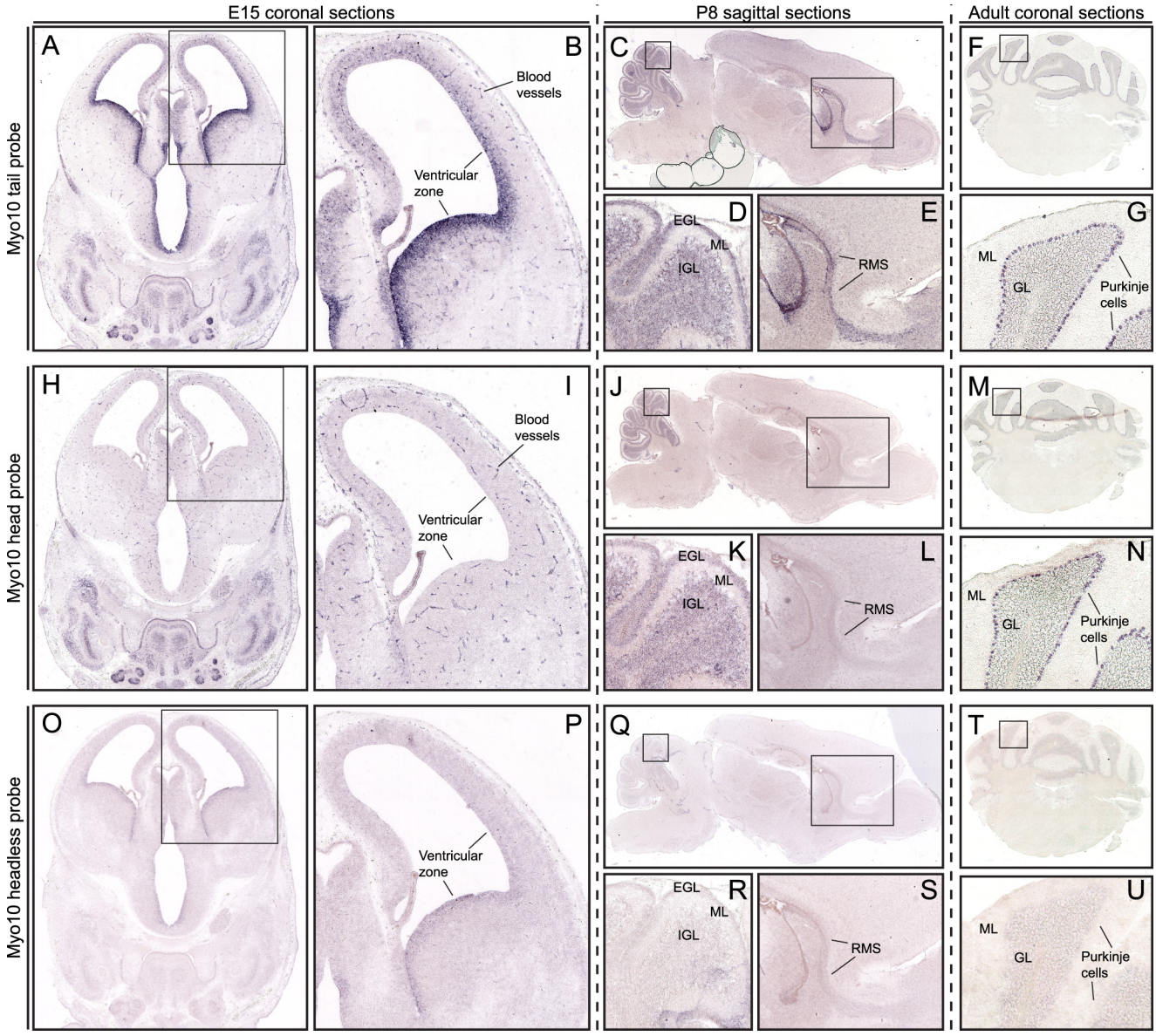


FIGURE 2. **Localization of full-length and headless Myo10 in the developing mouse brain.** Coronal sections of E15 mouse embryos (*left panels*), sagittal sections of P8 brains (*center panels*), and coronal sections of adult hindbrain (*right panels*), labeled with riboprobes to the tail region to detect both isoforms (*A–G*), the head region to detect full-length Myo10 (*H–N*), and the 5′ UTR of headless Myo10 to specifically detect headless Myo10 (*O–U*). In E15 brains, full-length Myo10 is most intensely expressed in blood vessels, whereas headless Myo10 is strongest in the ventricular zone. At P8, full-length Myo10 is strongly expressed in the external and internal granular layers of the cerebellum (*EGL* and *IGL*), whereas both isoforms appear to be expressed in the olfactory bulb, RMS, and the anterior portion of the ventricular zone. In the adult brain, full-length Myo10 is primarily expressed in Purkinje cells of the cerebellum. *EGL*, external granular layer, *IGL*, internal granular layer, *ML*, molecular layer, *GL*, granular layer.

ventricular zone of the embryonic brain (40). We also detect expression in the developing cortical plate and brain vasculature. Outside the brain, strong labeling is observed in the epithelium of the tongue and in muscle tissues.

The head probe shows similar labeling of non-neuronal tissues, but in the E15 brain, the strongest labeling is detected in blood vessels (Fig. 2, *H* and *I*). A weaker signal is detectable in the cortical plate. Because the tail probe strongly labels the ventricular zone but the head probe shows little to no signal in this region, we conclude that full-length Myo10 is primarily expressed in developing blood vessels and neurons, whereas headless Myo10 is most abundant in the ventricular zone. This conclusion is supported by the headless probe, which labels the ventricular zone, although it gives a weaker signal, probably because of its shorter length (Fig. 2, *O* and *P*).

Sagittal sections of P8 brain reveal continued expression of Myo10 in the cortical plate, where neurons at this stage are differentiating and forming synapses (Fig. 2*C*). However, Myo10 is expressed most strongly in two regions of active cell division and migration: the rostral migratory stream (RMS, Fig. 2*E*) and the external and internal granule cell layers of the cerebellum (*D*). Previous results with a probe to the tail of Myo10 also suggested that Myo10 is abundant in these regions at P7 (40). The external granule cell layer consists of granule cerebellar precursors undergoing rapid proliferation before migrating inwards to form the internal granular layer (42). Consistent

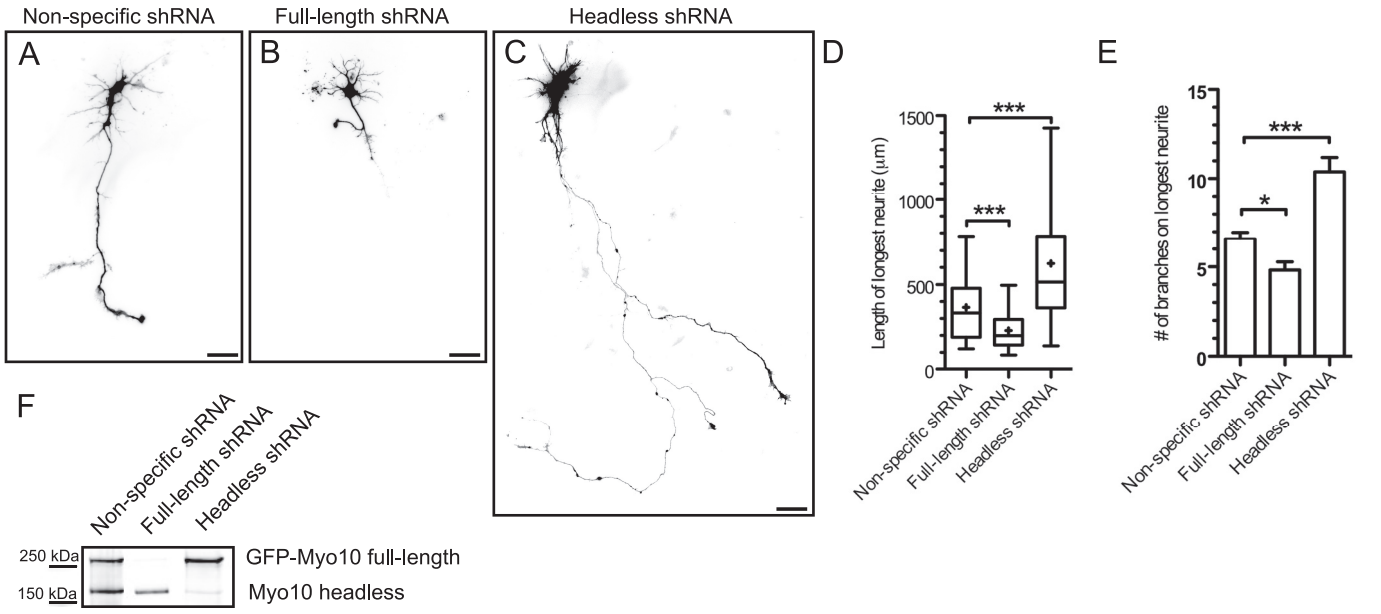


FIGURE 3. **Knockdown of full-length Myo10 inhibits axon outgrowth and branching, whereas knockdown of headless Myo10 increases axon outgrowth and branching.** To test the function of each isoform of Myo10, we developed shRNA constructs specific to each isoform and transfected them into cortical neurons. The neurons were dissociated from E15 cortex and cultured for 7 days. *A–C*, representative single neurons transfected with each shRNA and imaged at ×20 magnification. *Scale bars* = 30 μm. *D*, quantification of the length of the longest neurite on each neuron. *Whiskers*, 5–95%; *boxes*, 25–75%; *middle lines*, median; +, mean; ***, $p \leq 0.0001$. The means and S.E. are as follows: nonspecific shRNA, 366 ± 18 μm; full-length shRNA, 230 ± 15 μm; and headless shRNA, 624 ± 52 μm. *E*, quantification of the mean number of branches on the longest neurite of each neuron. *Error bars* represent mean ± S.E. *, indicates $p \leq 0.05$. The means and S.E. are as follows: nonspecific shRNA, 6.6 ± 0.4 branches; full-length shRNA, 4.83 ± 0.5 branches; and headless shRNA, 10.4 ± 0.8 branches. *F*, immunoblot of COS-7 cells cotransfected with GFP-full-length Myo10, headless Myo10, and the indicated shRNA. The full-length Myo10 shRNA targets the motor domain. The headless Myo10 shRNA targets the 5′ UTR, which is unique.

with our previous Western blotting results with mouse cerebellum (31), the tail and head probes, but not the headless probe, show strong labeling in the cerebellum, indicating expression of primarily full-length Myo10. The RMS is a population of neuronal precursors migrating from their birthplace in the subventricular zone to the olfactory bulb (43). The tail probe labels the RMS more strongly than the head probe, and the headless probe shows clear labeling of this region, indicating that Myo10 expression in the RMS is largely due to headless Myo10.

In adult brain sections, Myo10 is strongly expressed in the cerebellum, particularly in Purkinje cells (Fig. 2*F*), consistent with our previous blotting and *in situ* hybridization results (2, 31). This expression is detected by the head and tail probes, but not the headless probe, indicating that it is largely due to full-length Myo10 (Fig. 2).

*Knockdown of Full-length and Headless Myo10 Has Opposing Effects on Axon Outgrowth and Branching*—Because both isoforms of Myo10 are expressed in cortical neurons, we set out to determine the specific functions of full-length and headless Myo10 in neuronal development. We targeted full-length Myo10 for RNAi using a sequence from the motor domain (37) and utilized the unique 5′ UTR of headless Myo10 to specifically knock down headless Myo10 (Fig. 1*A*). shRNAs for these targets were cloned into a bicistronic vector expressing the shRNA under the RNA polymerase III-specific U6 promoter and Venus under the RNA polymerase II-specific chicken β-actin promoter (36). We confirmed specific knockdown in COS-7 cells cotransfected with both full-length and headless Myo10 (Fig. 3*F*).

We then tested these shRNA sequences in cortical neuron cultures and measured the effects on neuronal morphology. Cortices from E15 mice were electroporated with the shRNA constructs, dissociated, and the neurons grown in culture on poly-L-lysine and laminin for 7 days. To determine axon outgrowth, we measured the length and the number of branches on the longest neurite for each neuron. Knockdown of full-length Myo10 decreases axon outgrowth by ~37% compared with nonspecific shRNA (Fig. 3, *B* and *D*) and reduces branching by ~27% (*E*). Knockdown of headless Myo10 has opposing effects, nearly doubling axon outgrowth and increasing the number of branches by ~50% over control neurons (Fig. 3, *C–E*). Although knockdown of headless and full-length Myo10 had opposite effects on the total number of branches, we did not detect an effect on branch density. To confirm the specificity of these effects, we used a second set of shRNAs targeting headless and full-length Myo10, producing similar effects on axon morphology (supplemental Fig. S2).

*Overexpression of Full-length Myo10 Stimulates Axon Outgrowth and Branching, whereas Headless Myo10 Inhibits Axon Outgrowth and Branching*—Zhu *et al.* (28) reported that a motorless Myo10 construct suppressed axon outgrowth from cortical explants but that this construct only included amino acids 860–2062. Because endogenous headless Myo10 begins with Pro-645, it includes an additional 215 amino acids from the motor, IQ, and α-helical regions (Fig. 1*A*). We thus tested whether overexpression of the native headless Myo10 would inhibit axon outgrowth in cultured neurons. Using the same techniques to transfect and culture cortical neurons as in our knockdown experiments above, we determined that overexpression of GFP-tagged headless Myo10 indeed inhibits axon outgrowth by ~58% compared with GFP alone (Fig. 4, *C* and *D*).

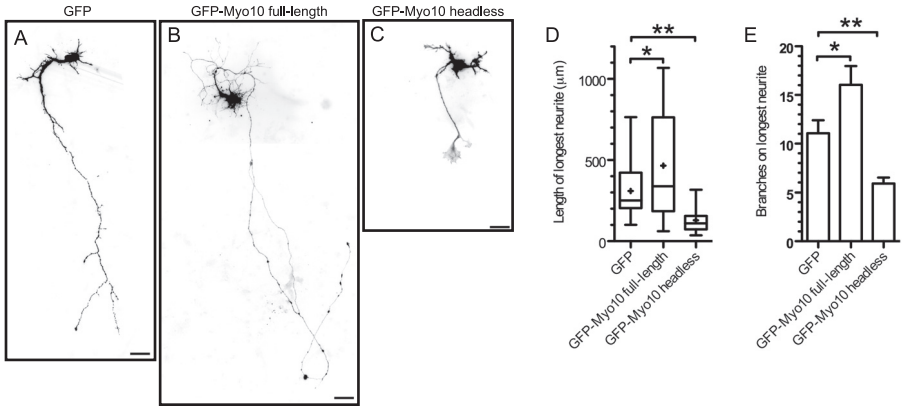


FIGURE 4. **Overexpression of full-length Myo10 stimulates axon outgrowth and branching, whereas headless Myo10 inhibits axon outgrowth and branching.** Neurons were transfected and cultured as in Fig. 3. *A–C*, representative neurons imaged at ×20. *Scale bars* = 30 μm. *D*, quantification of the length of the longest neurite on each neuron. *Whiskers*, 5–95%; *boxes*, 25–75%; *middle lines*, median; +, mean; *, indicates $p \leq 0.05$; **, $p \leq 0.001$. The means and S.E. are as follows: GFP, 309 ± 32 μm; GFP-Myo10 full-length, 465 ± 63 μm; and GFP-Myo10 headless, 129 ± 14 μm. *E*, quantification of the mean number of branches on the longest neurite of each neuron. *Error bars* = mean ± S.E. The means and S.E. are as follows: GFP, 10.7 ± 1.3 branches; GFP- Myo10 full-length, 16.0 ± 1.9 branches; GFP-Myo10 headless, and 5.91 ± 0.6 branches.

Overexpression of headless Myo10 also decreases branching by ~45% (Fig. 4, *C* and *E*).

On average, overexpression of full-length Myo10 increases both outgrowth and branching by ~50% (Fig. 4, *B* and *D*). However, neurons transfected with full-length Myo10 exhibit a broad range of axon lengths, and many have shorter axons than control neurons. These shorter axons are highly branched and may be associated with higher levels of expression of full-length Myo10 (supplemental Fig. S3), raising the possibility that full-length Myo10 promotes outgrowth at low levels but has deleterious effects at higher levels.

*Headless Myo10 Is a Negative Regulator of Full-length Myo10*—Since the discovery of headless Myo10, it has been widely hypothesized to function as an endogenous dominant negative of the full-length protein (28, 30, 31). This is consistent with our knockdown results showing opposite effects of full-length and headless Myo10 on axon outgrowth. To directly test whether headless Myo10 antagonizes full-length Myo10, we turned to a key function of full-length Myo10: filopodia induction. It has been shown previously that overexpression of full-length Myo10 in COS-7 cells increases the number of substrate-attached filopodia (5, 7, 10, 11, 27). Consistent with these previous studies, overexpression of full-length Myo10 led to a ~4-fold increase in substrate-attached filopodia (Fig. 5, *A* and *E*). On the other hand, overexpression of headless Myo10 has no significant effect on the baseline number of filopodia on COS-7 cells (Fig. 5*E*). However, coexpression of headless Myo10 with full-length Myo10 prevents the induction of filopodia by full-length Myo10 (Fig. 5, *B* and *E*), demonstrating that headless Myo10 can indeed antagonize the filopodia-inducing activity of full-length Myo10.

The structure of Myo10 suggests two mechanisms by which headless Myo10 may negatively regulate full-length Myo10. First, headless Myo10 may inhibit the activity of full-length Myo10 by forming heterodimers with only one motor domain. We and others have provided evidence that dimerization to form a two-headed motor is necessary for the motility of Myo10 on actin filaments (5, 7, 10, 44). Second, because headless Myo10 includes all of the tail domains of Myo10, the headless isoform might also act by competing for cargoes with full-length Myo10. Without any motor activity of its own, headless Myo10 could not transport these cargoes to their appropriate destinations. To test the first hypothesis, we coexpressed full-length Myo10 with the α-helical region of Myo10 (Fig. 5*D*), part of which forms a stable α-helix that lengthens the lever arm (45), whereas the remainder has been implicated in dimerization (5, 9, 10, 44). Coexpression of this α-helical region dramatically suppresses the induction of filopodia by full-length Myo10 (Fig. 5, *D* and *E*). To test the second hypothesis, we cotransfected full-length Myo10 with a Myo10 construct that includes the cargo-binding tail region but not the α-helical region (Fig. 5*C*), which also reduces the induction of filopodia (*C* and *E*). These results strongly suggest that headless Myo10 can antagonize full-length Myo10 both by dimerizing with full-length Myo10 and by sequestering cargoes away from the motor.

## DISCUSSION

In this study we have focused on headless Myo10, which lacks a functional motor domain, the defining feature of myosins. Headless Myo10 had been observed previously only in the nervous system, but its function had not been tested. We generated a shRNA specific to the 5′ UTR of headless Myo10 to determine the function of headless Myo10 in cortical neurons. Expression of this shRNA leads to dramatically increased axon outgrowth and branching, suggesting that headless Myo10 normally acts to inhibit these processes. Indeed, overexpression of headless Myo10 decreases axon outgrowth and branching, consistent with previous reports of decreased axon outgrowth using a shorter motorless Myo10 construct (28).

On the other hand, knockdown of full-length Myo10 decreases axon outgrowth and branching. This result suggests that previous data showing a requirement for Myo10 in commissural axon crossing in chick spinal cord (28) may reflect insufficient outgrowth rather than mistargeting of axons. Somewhat surprisingly, overexpression of full-length Myo10 does not uniformly produce longer axons but, rather, a broad range of axon lengths. This effect may be due to varying levels of

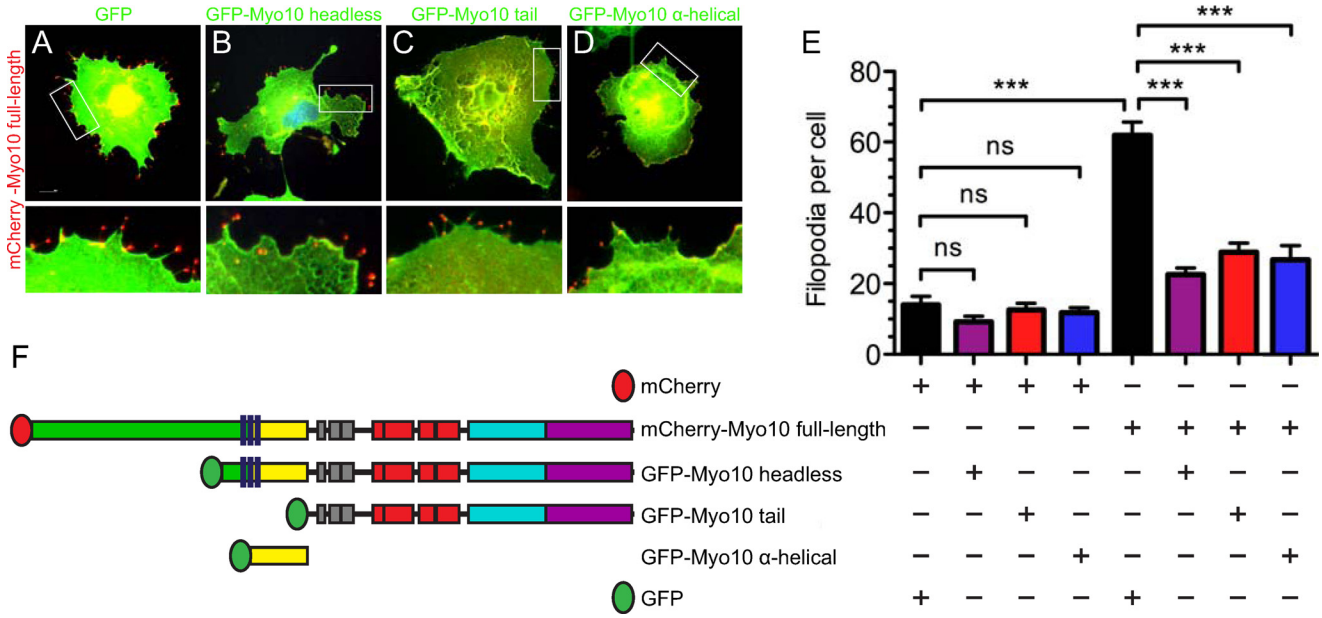


FIGURE 5. **Headless Myo10 is a negative regulator of full-length Myo10.** To test whether headless Myo10 antagonizes full-length Myo10, we measured filopodia induction in COS-7 cells grown on poly-L-lysine-coated glass. *A–D*, representative COS-7 cells transfected with mCherry-Myo10 full-length and either GFP (*A*), GFP-Myo10 headless (*B*), GFP-Myo10 tail (*C*), or GFP-Myo10 α-helical (*D*). *E*, quantification of substrate-attached filopodia/cell for cells transfected with the indicated constructs. *Error bars* = S.E. *ns*, not significant. ***, indicates $p < 0.0001$, $n \geq 40$ cells per condition. *F*, bar diagram of constructs used to transfect COS-7 cells.

overexpression. Too much full-length Myo10 may generate excess filopodia, aberrant branches, and shorter axons. Together, these results show that full-length Myo10 is required for protrusion of growth cones and branches, whereas headless Myo10 opposes the activity of full-length Myo10.

To directly demonstrate that headless Myo10 can antagonize full-length Myo10, we coexpressed the proteins in COS-7 cells and quantified the number of filopodia. Headless Myo10 indeed suppresses the induction of filopodia by full-length Myo10. Coexpression of the α-helical region also inhibits filopodia induction by full-length Myo10, and from this, we conclude that headless Myo10 likely dimerizes with full-length Myo10, forming a one-headed, two-tailed motor incapable of localizing to filopodia. Although a previous study showed that the α-helical region is sufficient to suppress dorsal filopodia in HeLa cells (11), in this study, expression of the α-helical region does not affect the number of substrate-attached filopodia on COS-7 cells at baseline. This difference may result from the small number of filopodia on control COS-7 cells (~14 substrate-attached filopodia/cell), whereas HeLa cells elaborate huge numbers of dorsal filopodia at baseline (~851 dorsal filopodia/cell) (11). Alternatively, the difference may reflect a fundamental distinction between dorsal and substrate-attached filopodia. Our results also show that the tail region of Myo10 is effective in counteracting filopodia induction by full-length Myo10, suggesting that headless Myo10 may compete with full-length Myo10 for binding partners.

So, if headless Myo10 is a negative regulator of full-length Myo10, what is the function of full-length Myo10 in growing axons? One obvious possibility is that full-length Myo10 is required for the formation or function of growth cone filopodia, which are crucial structures for growth cone motility and signaling (14). Filopodia are also key prerequisites for neurite initiation in cortical neurons (12). We do not detect a requirement for Myo10 in neurite initiation in our experiments, probably because knockdown of Myo10 does not occur until after neurites have formed. Future studies, perhaps utilizing genetic knockout of Myo10, will be needed to test whether Myo10 is required for neurite initiation.

Myo10 may also serve to transport cargoes within growth cone filopodia. Myo10 can bind to the netrin receptors DCC and neogenin (6, 23, 28, 29) and is required to localize DCC to neurites (28). However, in this study, outgrowth was not stimulated by any exogenous guidance cue or growth factor, indicating that Myo10 is required for baseline axon outgrowth independent of external cues.

The FERM domain of Myo10 can also bind β-integrins (27), adhesion molecules that mediate interactions with the extracellular matrix. Full-length Myo10 could couple these interactions to the actin cytoskeleton, a proposed mechanism for generating protrusive force at the leading edge (46). Full-length Myo10 can also link the actin and microtubule cytoskeletons with its motor and MyTH4 domains, respectively. Myo10 has been shown to mediate such interactions in mitotic and meiotic spindles (19–21), but it is unclear whether Myo10 participates in actin-microtubule interactions in growth cones. Because headless Myo10 lacks a functional motor domain, it cannot bind actin filaments, but it will be important to determine whether full-length Myo10 acts to link growth cone actin filaments to microtubules or integrins.

Our results also implicate Myo10 in axon branching. This is not surprising, as many of the cytoskeletal processes underlying axon outgrowth and guidance are shared with axon branching (47), including the importance of filopodia and actin-microtubule interactions (24). Another mechanism shared between these two processes is regulation by PI3K. This kinase is a con-

vergence point in axon guidance pathways, whereas localized activity of PI3K along the axon shaft forms patches of actin that precede axonal filopodia and, in turn, enlarge to become full-fledged branches (48). Recent *in vitro* work shows that Myo10 is autoinhibited until binding to the PI3K product phosphatidylinositol (3,4,5)-triphosphate (5), suggesting that Myo10 can link the PI3K pathway to the actin cytoskeleton.

Although we have shown that headless Myo10 can act as a negative regulator of full-length Myo10, we cannot exclude the possibility that headless Myo10 has functions independent of the full-length isoform. In fact, a gene with a domain structure remarkably similar to headless Myo10 was discovered in *Caenorhabditis elegans* (49). Loss of this gene, *max-1*, led to defects in motor axon guidance and decreased coordination. The MAX-1 protein, which includes the coiled-coil, PH, MyTH4 and FERM domains, appeared to participate in netrin-mediated axon repulsion. Recent evidence suggests that, in vertebrates, the primary function of MAX-1 may be in angiogenesis (50). These studies suggest future avenues for investigation of headless Myo10.

The expression pattern we observed in this study also suggests novel and unexpected functions for Myo10. Our immunoblotting and *in situ* hybridization reveal that headless Myo10 is expressed in the developing mouse cortex in neurons and astrocytes but is also abundant in neural stem cells. Although full-length Myo10 is also detected in neural stem cells, Myo10 expression in the embryonic ventricular zone and the postnatal rostral migratory stream appears to be primarily due to headless Myo10. This suggests a new and surprising role for headless Myo10 in neurogenesis. A number of studies have identified a role for full-length Myo10 in mitotic and meiotic spindles (20, 21), including integrin-dependent spindle orientation (19). Spindle orientation is thought to be important for cell fate determination in neural progenitor mitosis (51, 52), and $\beta$1-integrin adhesion is required for normal neurogenesis in this cell population (53). Headless Myo10 has not been previously associated with spindle function, but the strong expression in the ventricular zone suggests that it may be important for neurogenesis, and further work is warranted to test this possibility.

We were also intrigued to find that in the embryonic brain, full-length Myo10 strongly labels the developing vasculature, raising the possibility of a role for Myo10 in angiogenesis. A previous study found a requirement for Myo10 in guiding endothelial migration toward a BMP6 gradient (37), so it will be important to test whether Myo10 participates in endothelial cell migration and angiogenesis *in vivo*.

Myo10 has been shown to function in migration of another cell type *in vivo*: cranial neural crest cells (54, 55). Morpholino-mediated knockdown of Myo10 during early *Xenopus laevis* development slowed neural crest cell migration and impaired the formation of pharyngeal arch structures. Myo10 knockdown also decreased filopodia and adhesions when the cells were cultured *in vitro*. Similarly, experiments with NLT cells, a neuronal cell line, showed that overexpression of a motorless Myo10 construct decreased migration and focal adhesion formation (30). The enrichment of Myo10 that we observed in the rostral migratory stream of the postnatal brain suggests that Myo10 may be important for the migration of some populations of neurons in the brain.

Finally, given the importance of filopodia in dendritic spine formation (56, 57), it will be important to investigate the role of Myo10 in dendritic spines. Future studies of the functions of Myo10 in the nervous system would benefit greatly from a genetic knockout of Myo10, but, given the distinct and opposing functions of full-length and headless Myo10 outlined in this study, it will also be important to selectively delete the headless isoform. This would allow determination of the *in vivo* functions of this unusual isoform. Investigating the role of headless Myo10 in stem cells will be of particular interest.

*Acknowledgments—We thank the Confocal and Multiphoton Imaging and the In Situ Hybridization core facilities of the UNC Neuroscience Center and the UNC Proteomics Core Facility for technical assistance, Rick Meeker for providing astrocytes, Victoria Bautch for embryonic stem cell cultures, Brian D. Dunn for help making constructs, and Franck Polleux and Julien Courchet for advice and technical assistance.*

## REFERENCES

1. Kerber, M. L., and Cheney, R. E. (2011) Myosin-X. A MyTH-FERM myosin at the tips of filopodia. *J. Cell Sci.* **124,** 3733–3741
2. Berg, J. S., Derfler, B. H., Pennisi, C. M., Corey, D. P., and Cheney, R. E. (2000) Myosin-X, a novel myosin with pleckstrin homology domains, associates with regions of dynamic actin. *J. Cell Sci.* **113,** 3439–3451
3. Bennett, R. D., Mauer, A. S., and Strehler, E. E. (2007) Calmodulin-like protein increases filopodia-dependent cell motility via up-regulation of myosin-10. *J. Biol. Chem.* **282,** 3205–3212
4. Plantard, L., Arjonen, A., Lock, J. G., Nurani, G., Ivaska, J., and Strömblad, S. (2010) PtdIns(3,4,5)P; is a regulator of myosin-X localization and filopodia formation. *J. Cell Sci.* **123,** 3525–3534
5. Umeki, N., Jung, H. S., Sakai, T., Sato, O., Ikebe, R., and Ikebe, M. (2011) Phospholipid-dependent regulation of the motor activity of myosin X. *Nat. Struct. Mol. Biol.* **18,** 783–788
6. Liu, Y., Peng, Y., Dai, P. G., Du, Q. S., Mei, L., and Xiong, W. C. (2012) Differential regulation of myosin X movements by its cargos, DCC and neogenin. *J. Cell Sci.* **125,** 751–762
7. Berg, J. S., and Cheney, R. E. (2002) Myosin-X is an unconventional myosin that undergoes intrafilopodial motility. *Nat. Cell Biol.* **4,** 246–250
8. Almagro, S., Durmort, C., Chervin-Pétinot, A., Heyraud, S., Dubois, M., Lambert, O., Maillefaud, C., Hewat, E., Schaal, J. P., Huber, P., and Gulino-Debrac, D. (2010) The motor protein myosin-X transports VE-cadherin along filopodia to allow the formation of early endothelial cell-cell contacts. *Mol. Cell. Biol.* **30,** 1703–1717
9. Kerber, M. L., Jacobs, D. T., Campagnola, L., Dunn, B. D., Yin, T., Sousa, A. D., Quintero, O. A., and Cheney, R. E. (2009) A novel form of motility in filopodia revealed by imaging myosin-X at the single-molecule level. *Curr. Biol.* **19,** 967–973
10. Tokuo, H., Mabuchi, K., and Ikebe, M. (2007) The motor activity of myosin-X promotes actin fiber convergence at the cell periphery to initiate filopodia formation. *J. Cell Biol.* **179,** 229–238
11. Bohil, A. B., Robertson, B. W., and Cheney, R. E. (2006) Myosin-X is a molecular motor that functions in filopodia formation. *Proc. Natl. Acad. Sci. U.S.A.* **103,** 12411–12416
12. Dent, E. W., Kwiatkowski, A. V., Mebane, L. M., Philippar, U., Barzik, M., Rubinson, D. A., Gupton, S., Van Veen, J. E., Furman, C., Zhang, J., Alberts, A. S., Mori, S., and Gertler, F. B. (2007) Filopodia are required for cortical neurite initiation. *Nat. Cell Biol.* **9,** 1347–1359
13. Dent, E. W., Gupton, S. L., and Gertler, F. B. (2011) The growth cone cytoskeleton in axon outgrowth and guidance. *Cold Spring Harb. Perspect. Biol.* **3,** 1–39
14. Drees, F., and Gertler, F. B. (2008) Ena/VASP. Proteins at the tip of the

nervous system. *Curr. Opinion Neurobiol.* **18,** 53–59
15. Mattila, P. K., and Lappalainen, P. (2008) Filopodia. Molecular architecture and cellular functions. *Nat. Rev. Mol. Cell Biol.* **9,** 446–454
16. Tanabe, K., Bonilla, I., Winkles, J. A., and Strittmatter, S. M. (2003) Fibroblast growth factor-inducible-14 is induced in axotomized neurons and promotes neurite outgrowth. *J. Neurosci.* **23,** 9675–9686
17. Mashanov, G. I., Tacon, D., Peckham, M., and Molloy, J. E. (2004) The spatial and temporal dynamics of pleckstrin homology domain binding at the plasma membrane measured by imaging single molecules in live mouse myoblasts. *J. Biol. Chem.* **279,** 15274–15280
18. Cox, D., Berg, J. S., Cammer, M., Chinegwundoh, J. O., Dale, B. M., Cheney, R. E., and Greenberg, S. (2002) Myosin X is a downstream effector of PI(3)K during phagocytosis. *Nat. Cell Biol.* **4,** 469–477
19. Toyoshima, F., and Nishida, E. (2007) Integrin-mediated adhesion orients the spindle parallel to the substratum in an EB1- and myosin X-dependent manner. *EMBO J.* **26,** 1487–1498
20. Weber, K. L., Sokac, A. M., Berg, J. S., Cheney, R. E., and Bement, W. M. (2004) A microtubule-binding myosin required for nuclear anchoring and spindle assembly. *Nature* **431,** 325–329
21. Woolner, S., O'Brien, L. L., Wiese, C., and Bement, W. M. (2008) Myosin-10 and actin filaments are essential for mitotic spindle function. *J. Cell Biol.* **182,** 77–88
22. Woolner, S., and Papalopulu, N. (2012) Spindle position in symmetric cell divisions during epiboly is controlled by opposing and dynamic apicobasal forces. *Dev. Cell* **22,** 775–787
23. Hirano, Y., Hatano, T., Takahashi, A., Toriyama, M., Inagaki, N., and Hakoshima, T. (2011) Structural basis of cargo recognition by the myosin-X MyTH4-FERM domain. *EMBO J.* **30,** 2734–2747
24. Dent, E. W., and Kalil, K. (2001) Axon branching requires interactions between dynamic microtubules and actin filaments. *J. Neurosci.* **21,** 9757–9769
25. Geraldo, S., and Gordon-Weeks, P. R. (2009) Cytoskeletal dynamics in growth-cone steering. *J. Cell Sci.* **122,** 3595–3604
26. Kalil, K., and Dent, E. W. (2005) Touch and go. Guidance cues signal to the growth cone cytoskeleton. *Curr. Opin. Neurobiol.* **15,** 521–526
27. Zhang, H., Berg, J. S., Li, Z., Wang, Y., Lång, P., Sousa, A. D., Bhaskar, A., Cheney, R. E., and Strömblad, S. (2004) Myosin-X provides a motor-based link between integrins and the cytoskeleton. *Nat. Cell Biol.* **6,** 523–531
28. Zhu, X. J., Wang, C. Z., Dai, P. G., Xie, Y., Song, N. N., Liu, Y., Du, Q. S., Mei, L., Ding, Y. Q., and Xiong, W. C. (2007) Myosin X regulates netrin receptors and functions in axonal path-finding. *Nat. Cell Biol.* **9,** 184–192
29. Wei, Z., Yan, J., Lu, Q., Pan, L., and Zhang, M. (2011) Cargo recognition mechanism of myosin X revealed by the structure of its tail MyTH4-FERM tandem in complex with the DCC P3 domain. *Proc. Natl. Acad. Sci. U.S.A.* **108,** 3572–3577
30. Wang, J. J., Fu, X. Q., Guo, Y. G., Yuan, L., Gao, Q. Q., Yu, H. L., Shi, H. L., Wang, X. Z., Xiong, W. C., and Zhu, X. J. (2009) Involvement of headless myosin X in the motility of immortalized gonadotropin-releasing hormone neuronal cells. *Cell Biol. Int.* **33,** 578–585
31. Sousa, A. D., Berg, J. S., Robertson, B. W., Meeker, R. B., and Cheney, R. E. (2006) Myo10 in brain. Developmental regulation, identification of a headless isoform and dynamics in neurons. *J. Cell Sci.* **119,** 184–194
32. Polleux, F., and Ghosh, A. (2002) The slice overlay assay. A versatile tool to study the influence of extracellular signals on neuronal development. *Sci. STKE* **136,** 19
33. Barnes, A. P., Lilley, B. N., Pan, Y. A., Plummer, L. J., Powell, A. W., Raines, A. N., Sanes, J. R., and Polleux, F. (2007) LKB1 and SAD kinases define a pathway required for the polarization of cortical neurons. *Cell* **129,** 549–563
34. Hutton, S. R., and Pevny, L. H. (2008) Isolation, culture, and differentiation of progenitor cells from the central nervous system. *CSH Protoc* **11,** 1029–1033
35. Popko, J., Fernandes, A., Brites, D., and Lanier, L. M. (2009) Automated analysis of NeuronJ tracing data. *Cytometry* **75,** 371–376
36. Hand, R., and Polleux, F. (2011) Neurogenin2 regulates the initial axon guidance of cortical pyramidal neurons projecting medially to the corpus callosum. *Neural Dev.* **6,** 30
37. Pi, X., Ren, R., Kelley, R., Zhang, C., Moser, M., Bohil, A. B., Divito, M., Cheney, R. E., and Patterson, C. (2007) Sequential roles for myosin-X in BMP6-dependent filopodial extension, migration, and activation of BMP receptors. *J. Cell Biol.* **179,** 1569–1582
38. Hand, R., Bortone, D., Mattar, P., Nguyen, L., Heng, J. I., Guerrier, S., Boutt, E., Peters, E., Barnes, A. P., Parras, C., Schuurmans, C., Guillemot, F., and Polleux, F. (2005) Phosphorylation of Neurogenin2 specifies the migration properties and the dendritic morphology of pyramidal neurons in the neocortex. *Neuron* **48,** 45–62
39. Lein, E. S., Hawrylycz, M. J., Ao, N., Ayres, M., Bensinger, A., Bernard, A., Boe, A. F., Boguski, M. S., Brockway, K. S., Byrnes, E. J., Chen, L., Chen, L., Chen, T. M., Chin, M. C., Chong, J., Crook, B. E., Czaplinska, A., Dang, C. N., Datta, S., Dee, N. R., Desaki, A. L., Desta, T., Diep, E., Dolbeare, T. A., Donelan, M. J., Dong, H. W., Dougherty, J. G., Duncan, B. J., Ebbert, A. J., Eichele, G., Estin, L. K., Faber, C., Facer, B. A., Fields, R., Fischer, S. R., Fliss, T. P., Frensley, C., Gates, S. N., Glattfelder, K. J., Halverson, K. R., Hart, M. R., Hohmann, J. G., Howell, M. P., Jeung, D. P., Johnson, R. A., Karr, P. T., Kawal, R., Kidney, J. M., Knapik, R. H., Kuan, C. L., Lake, J. H., Laramee, A. R., Larsen, K. D., Lau, C., Lemon, T. A., Liang, A. J., Liu, Y., Luong, L. T., Michaels, J., Morgan, J. J., Morgan, R. J., Mortrud, M. T., Mosqueda, N. F., Ng, L. L., Ng, R., Orta, G. J., Overly, C. C., Pak, T. H., Parry, S. E., Pathak, S. D., Pearson, O. C., Puchalski, R. B., Riley, Z. L., Rockett, H. R., Rowland, S. A., Royall, J. J., Ruiz, M. J., Sarno, N. R., Schaffnit, K., Shapovalova, N. V., Sivisay, T., Slaughterbeck, C. R., Smith, S. C., Smith, K. A., Smith, B. I., Sodt, A. J., Stewart, N. N., Stumpf, K. R., Sunkin, S. M., Sutram, M., Tam, A., Teemer, C. D., Thaller, C., Thompson, C. L., Varnam, L. R., Visel, A., Whitlock, R. M., Wohnoutka, P. E., Wolkey, C. K., Wong, V. Y., Wood, M., Yaylaoglu, M. B., Young, R. C., Youngstrom, B. L., Yuan, X. F., Zhang, B., Zwingman, T. A., and Jones, A. R. (2007) Genome-wide atlas of gene expression in the adult mouse brain. *Nature* **445,** 168–176
40. Magdaleno, S., Jensen, P., Brumwell, C. L., Seal, A., Lehman, K., Asbury, A., Cheung, T., Cornelius, T., Batten, D. M., Eden, C., Norland, S. M., Rice, D. S., Dosooye, N., Shakya, S., Mehta, P., and Curran, T. (2006) BGEM. An *in situ* hybridization database of gene expression in the embryonic and adult mouse nervous system. *PLoS Biol.* **4,** e86
41. Visel, A., Thaller, C., and Eichele, G. (2004) GenePaint.org. An atlas of gene expression patterns in the mouse embryo. *Nucleic Acids Res.* **32,** D552–556
42. Roussel, M. F., and Hatten, M. E. (2011) Cerebellum development and medulloblastoma. *Curr. Top. Dev. Biol.* **94,** 235–282
43. Kriegstein, A., and Alvarez-Buylla, A. (2009) The glial nature of embryonic and adult neural stem cells. *Annu. Rev. Neurosci.* **32,** 149–184
44. Nagy, S., and Rock, R. S. (2010) Structured post-IQ domain governs selectivity of myosin X for fascin-actin bundles. *J. Biol. Chem.* **285,** 26608–26617
45. Knight, P. J., Thirumurugan, K., Xu, Y., Wang, F., Kalverda, A. P., Stafford, W. F., 3rd, Sellers, J. R., and Peckham, M. (2005) The predicted coiled-coil domain of myosin 10 forms a novel elongated domain that lengthens the head. *J. Biol. Chem.* **280,** 34702–34708
46. Suter, D. M., and Forscher, P. (2000) Substrate-cytoskeletal coupling as a mechanism for the regulation of growth cone motility and guidance. *J. Neurobiol.* **44,** 97–113
47. Kalil, K., Szebenyi, G., and Dent, E. W. (2000) Common mechanisms underlying growth cone guidance and axon branching. *J. Neurobiol.* **44,** 145–158
48. Ketschek, A., and Gallo, G. (2010) Nerve growth factor induces axonal filopodia through localized microdomains of phosphoinositide 3-kinase activity that drive the formation of cytoskeletal precursors to filopodia. *J. Neurosci.* **30,** 12185–12197
49. Huang, X., Cheng, H. J., Tessier-Lavigne, M., and Jin, Y. (2002) MAX-1, a novel PH/MyTH4/FERM domain cytoplasmic protein implicated in netrin-mediated axon repulsion. *Neuron* **34,** 563–576
50. Zhong, H., Wu, X., Huang, H., Fan, Q., Zhu, Z., and Lin, S. (2006) Vertebrate MAX-1 is required for vascular patterning in zebrafish. *Proc. Natl. Acad. Sci. U.S.A.* **103,** 16800–16805
51. Knoblich, J. A. (2008) Mechanisms of asymmetric stem cell division. *Cell* **132,** 583–597

52. Postiglione, M. P., Jüschke, C., Xie, Y., Haas, G. A., Charalambous, C., and Knoblich, J. A. (2011) Mouse inscuteable induces apical-basal spindle orientation to facilitate intermediate progenitor generation in the developing neocortex. *Neuron* **72,** 269–284
53. Loulier, K., Lathia, J. D., Marthiens, V., Relucio, J., Mughal, M. R., Tang, S. C., Coksaygan, T., Hall, P. E., Chigurupati, S., Patton, B., Colognato, H., Rao, M. S., Mattson, M. P., Haydar, T. F., and Ffrench-Constant, C. (2009) $\beta$1 Integrin maintains integrity of the embryonic neocortical stem cell niche. *PLoS Biol.* **7,** e1000176
54. Hwang, Y. S., Luo, T., Xu, Y., and Sargent, T. D. (2009) Myosin-X is required for cranial neural crest cell migration in *Xenopus laevis*. *Dev. Dyn.* **238,** 2522–2529
55. Nie, S., Kee, Y., and Bronner-Fraser, M. (2009) Myosin-X is critical for migratory ability of *Xenopus* cranial neural crest cells. *Dev. Biol.* **335,** 132–142
56. Dent, E. W., Merriam, E. B., and Hu, X. (2011) The dynamic cytoskeleton. Backbone of dendritic spine plasticity. *Curr. Opin. Neurobiol.* **21,** 175–181
57. Hotulainen, P., and Hoogenraad, C. C. (2010) Actin in dendritic spines. Connecting dynamics to function. *J. Cell Biol.* **189,** 619–629